THERMAL AND FLOW MIXING ANALYSIS IN A SQUARE HOT WATER STORAGE TANK DURING DISCHARGE USING PIV/PLIF TECHNIQUES

Liqun SHAO[1], Jingjin LI[1], Hongkai FU[1], Kun LIU[1], Wenfeng GAO[1*], Qiong LI[1*]

[1]Yunnan Provincial Key Laboratory of Rural Energy Engineering, Yunnan Normal University, Kunming, Yunnan 650500, China

[*] Corresponding author; E-mail: wenfenggao@163.com; liqiong@ynnu.edu.cn

The square-shaped hot water storage tank is widely used in thermal energy storage systems due to its easy processing and installation. In this study, to address the degradation of water discharge efficiency caused by the mixing of cold and hot water in the hot water discharge process of square tanks, based on modelling experiments, particle image velocimetry and laser-induced fluorescence techniques were used to visualise and quantitatively analyse the thermal mixing phenomenon in a conventional square hot water storage tank with typical water discharge flow rate in engineering applications (940 ⩽ Re ⩽ 3290) and in the tanks with three different outlet positions. A detailed visualisation and quantitative analysis of the hot and cold water mixing phenomenon in the storage tank was carried out. The experimental results show that the maximum vortex height (h_v) formed by the jet gradually increases with the increase of Re at the inlet, and the jet has stronger entrainment and mixing effects. Compared with the effect of Re, the jet-induced entrainment and mixing with the effect of different hot water outlet positions (h_0/l) are relatively small. When the h_0/l is 1/2, a noticeable temperature stratification occurs for 940 ⩽ Re ⩽ 1880,. For 2350 ⩽ Re ⩽ 3290, the stratification weakens, and the mixing between the jet and the surrounding fluid becomes more intense, resulting in a broader distribution of the thermocline. The results of the study can provide a reference for optimising the energy-saving design of the square hot water storage tank.

Keywords: *Square hot water storage tank; Mixing Characteristics; PIV/PLIF; Inlet Re number; Height of hot water outlet*

1. Introduction

As a critical device for charging and discharging thermal energy, hot water storage tanks are widely used in industrial and agricultural applications and in human daily life, such as in electric heating, heat pump and solar water heating systems in hotels, restaurants, schools, hospitals and households [1, 2]. The structural design of the storage tank is not only related to the efficiency of thermal energy utilisation, but also directly affects the overall operational efficiency of the system [3, 4]. In some large-scale hot water projects, square-shaped hot water storage tanks are widely used due to their compact structure, easy on-site processing, installation and maintenance. Due to the multifaceted and rectangular structural characteristics, the mixing process of cold water and hot water during discharge is complicated, which not only affects the hot water discharge efficiency of the storage tank, but also aggravates the uneven temperature distribution and affects the heat storage and discharge performance of the storage tank. When the cold water flows into the tank at a higher velocity, its negative buoyancy properties cause the jet to deflect downward, resulting in a complex flow pattern. This process is one of the primary mechanisms for thermal mixing [5]. Therefore, an in-depth study of the behavior of cold water inlet jets is of great significance for optimizing the design of storage tanks and improving the efficiency of thermal energy utilization.

Regarding jet flow studies in the thermal storage tank discussed herein, Philippe et al. [6] thoroughly investigated the penetration behaviour of negatively buoyant jets (*Re* = 940 to 3290) in miscible fluid bodies through a combination of experiments and theoretical models. Their proposed theoretical model was based on fluid dynamics and successfully predicted the transient and steady state penetration distances of the jet. Qin et al. [7] carried out an experimental study of buoyant jets in a two-layer stratified environment inside a square tank under high *Re* conditions using the PIV/PLIF technique. The variation rules of the mean velocity distribution and the jet penetration depth were analysed. Van Berkel et al. [8, 9] employed a combination of theoretical analysis, numerical simulation, and experimental validation to thoroughly investigate the thermal mixing phenomena and dynamic characteristics in two-layer stratified storage systems, with particular emphasis on the critical role of Kelvin-Helmholtz instabilities in the mixing within the thermocline zone. They proposed analytical models and numerical simulation methods to optimize the design and operation of storage tanks. Pablo et al. [10] introduced the Virtual TC method in their study, which combines 5PL functions and spline interpolation techniques to accurately estimate the instantaneous temperature distribution and thermocline thickness during the charging process of hot water storage tanks. This approach provides a comprehensive evaluation of the tank's thermal performance. Haddouche et al. [11] developed a one-dimensional numerical model of a stratified hot water storage tank using the finite difference method, validated through experimental tests following EN16147 standards. The model captured transient temperature distributions during charging/discharging processes and reduced cooling time prediction error by approximately 5% compared to existing models. In this study, the fluid is injected horizontally, with its initial momentum direction perpendicular to the direction of gravity, differing from traditional negative buoyancy jets. We term this phenomenon the "horizontally injected momentum-buoyancy coupled jet," or simply cross buoyancy jet, to highlight this unique interaction between momentum and buoyancy.

The location of the inlet and outlet of a hot water storage tank also has a significant effect on the mixing mechanism and thermal stratification in the storage tank. El-Amin et al. [12-14] conducted an in-depth study on the turbulence and heat transfer of a cold shower flow into a solar energy storage tank through experimental and numerical analyses and demonstrated experimentally measured and numerically simulated results of a two-dimensional axisymmetric vertical thermal jet flow into a cylindrical water storage tank with constant or variable inlet temperatures. Secondly, the cold water inlet flow rate and hot water outlet flow rate are key parameter affecting system performance. This involves studying the mixing characteristics of hot and cold water in the thermal storage tank under different inlet and outlet *Re*. Chandra et al [15] numerically investigated the effect of inlet conditions on thermal stratification in the discharge process. They investigated different inlet conditions including simple inlet, slotted inlet and perforated inlet with some dimensionless numbers (e.g. *Re* and *Ri*) for interpretation and showed that the effect of inlet conditions on the degree of stratification depends on the flow rate. Assari et al [16, 17] carried out a detailed experimental and numerical study on the effect of inlet and outlet positions on the optimization of the thermal stratification process in a horizontal cylindrical storage tank. A key finding of their study was that the location of the hot water inlet has a significant effect on the thermal stratification effect. When the hot water flows from the highest position, the thermal stratification effect is significantly improved due to the reduced mixing with the cold water in the tank. Li et al [18] explored the thermal performance of solar water storage tanks with variable inlet and outlet configurations, utilizing CFD simulations alongside theoretical analysis. They proposed two new charging strategies aimed at mitigate temperature mixing associated with outlet switching. Additionally, these strategies optimize thermal stratification by dynamically adjusting the inlet position to a suitable height, thereby enhancing the overall efficiency of the storage system.

Square water storage tanks play an important role in large-scale solar water heating systems, industrial and agricultural heat utilisation and other occasions. Compared with the common cylindrical hot water storage tank, the multilateral and inlet/outlet structure of the square tank have a more obvious effect on the mixing of hot and cold water. However, there are fewer studies on the thermal mixing phenomenon caused by cross buoyant jets in square tanks and the position of the inlet and outlet of the tank. Therefore, this paper uses PIV and PLIF measurement techniques to experimentally study and analyse the water mixing characteristics of a square storage tank under drainage conditions, to reveal the transient flow dynamics of the horizontal cross buoyant jet at the inlet of the square tank, and to explore the influence of the outlet position on the mixing of hot and cold water. To provide a scientific and reasonable design basis for the optimisation of hot water storage tank structure.

2. Method

2.1. Experimental instrumentation

In this paper, a large square hot water storage tank (length: 1.7m, width: 1.7m, height: 2.4m), commonly used in solar water heating projects, is adopted as the prototype for the study. The tank is a non-pressurized one, with an opening at the top designed for easy maintenance. The cold water inlet is located at the bottom of one side of the tank, with a flow rate ranging from 227 L/h to 794 L/h, while the hot water outlet is positioned at the top of the opposite side. Since PIV/PLIF cannot directly measure the thermal mixing and flow structure caused by horizontal cross buoyant jets inside a large square hot water storage tank, this study employed a model theory to scale down the tank by 5.7 times. The experimental tank maintains the same height-to-width ratio as the actual hot water tank. The inlet and outlet are circular tubes with a diameter of 0.015 m. The cold water inlet is positioned 0.05 m above the tank bottom, while the three hot water outlets are located 0.0525 m, 0.14 m, and 0.21 m above the tank bottom, respectively, to evaluate the impact of different outlet heights on mixing characteristics. The *Re*, defined in equation (1), was selected as the determining dimensionless parameter based on model theory, a method commonly used in experiments studying jet flow fields in tanks [19, 20].

$$Re = \frac{V_y D_y}{\nu} = \frac{VD}{\nu} \tag{1}$$

Where V is the jet velocity of the model, D is the hydraulic diameter of the model, and ν is the kinematic viscosity of the fluid at the inlet temperature (T_0=20℃, ν=1.004×10^{-6}m^2/s). For the full-scale prototype (actual hot water storage tank), V_y is the inlet flow velocity of the actual hot water storage tank, and D_y represents its hydraulic diameter.

To study the thermal mixing effect of cross buoyant jets in hot water storage tanks, an experimental platform was built and tested using PIV/PLIF, as shown in Figure 1. The experimental platform mainly consists of experimental devices (hot water tank, cold water tank and make-up tank), velocity/temperature measurement system, control devices (stirrer, flow meter and valve, etc.) and related pipelines. The measuring range and accuracy of each component of the experimental equipment are listed in Table 1.

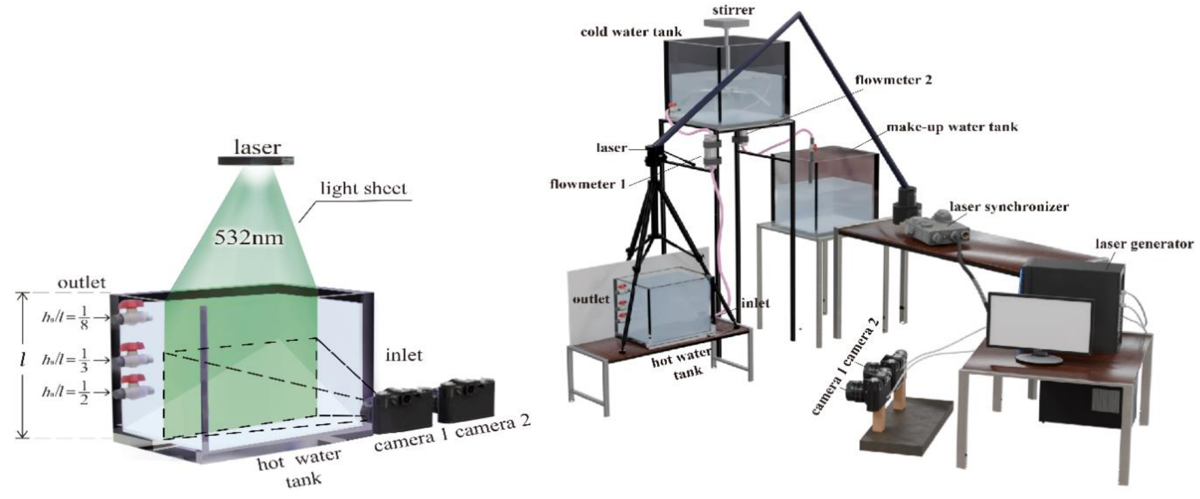

(a) **Square experimental water tank** (b) **PIV/PLIF Testing System**

Figure 1. Experimental platform

Table 1. Details of the measurement system and their measurement range and accuracy

System Configuration	Model	Measurement Range and Accuracy
PIV/LIF flow field measurement system (LaVision, Germany)		
Dual-cavity Laser	Dual-pulse Nd: YAG laser	Laser wavelength 532nm, Pulse energy 400mJ, Pulse width 4ns, Frequency 15HZ
Synchronous Controller	Nano L200-15	—
Dual CCD Cameras	Imager sCMOS	Resolution 1600 × 1200 pixels, F = 50/1.8
Aftertreatment System	DaVis8.4	—
Flow Field Configuration Components		
Test Tank	Transparent Tempered Glass Tank	0.3×0.3×0.42m, Thickness 0.007m
Refueling Tank	Transparent Plexiglass Tank	0.5×0.5×0.5m, Thickness 0.007m
Cold Water Tank	Transparent Plexiglass Tank	0.5×0.5×0.5m, Thickness 0.007m
Water Pump	HQB-300	Rated supply: 220~240VAC/50HZ, Rated power: 70W Maximum head: 3m, Maximum flow: 2500L/H
Thermometer	Glass Bar Type	Range: 0-100℃, Accuracy: 1℃
Electric Heating Tube	A7-2	Rated supply: 220V~50Hz, Rated power: 1500W

2.2. PIV experimental method

The experiment used a double-pulse laser as the laser light source, through the light guide arm and sheet laser formers to produce 532nm laser pulse sheet light source, forming a thickness of about 1mm surface laser. The laser plane is positioned on the vertical plane passing through the centers of the inlet and outlet to accurately capture velocity and temperature field information. The laser intensity was set at 20% and the laser frequency at 15 Hz. The light source vertically illuminated the tracer particles in the test tank, and the scattered light reached the CCD camera outside the flow field. The CCD camera captured 800 images in double - frame and double - exposure mode. These images were then processed by the system's post - processing software with a query window set to 32×32 pixels. In the following text, the time - averaged velocity refers to the average velocity over 1 second (equivalent to 15 images).The relevant settings for the PIV and PLIF experiments are shown in Table 2.

Table 2. Settings for PIV and PLIF experiments

Types of Experiments	Camera1 filters	Camera2 filters	Tracer Particles	Parameters
PIV	532nm	532nm	Hollow Glass Sphere	Diameter 10μm, Density 1.1g/cm^3
PLIF	600nm	550nm	Rhodamine B Rhodamine 110	$\lambda_{a,max}$=560nm, $\lambda_{e,max}$ =585nm $\lambda_{a,max}$=496nm, $\lambda_{e,max}$ =520nm

2.3. PLIF experimental method

The PLIF experiment uses the LIF two-color method of temperature measurement module. In principle, one of the dyes should be sensitive to temperature, while the other should be insensitive or just very weak. The two-color method eliminates the dependence of the laser intensity on the detection volume. In addition, the emission spectra of the two dyes should be sufficiently different to optically separate the emitted light [21].The technique of two-color laser-induced fluorescence applied to temperature measurements in liquid flows is based on the measurement of the fluorescence intensity of dye tracers added to the fluid. Especially in liquids, fluorescence emission is strongly affected by bursting, which is a temperature dependent process. The dependence of fluorescence intensity on temperature can be expressed by the equation [22]:

$$ln(R_f / R_{f,ref}) = A(1/T^2 - 1/T_{ref}^2) + B(1/T - 1/T_{ref}) \tag{2}$$

where $ln(R_f / R_{f,ref})$ can be measured and plotted for intensities at different temperatures. The above equation should then be fitted to the data to calculate the values of A and B from the calibration curve. The temperature of the system can then be calculated from the intensity ratios obtained and the calibration parameters A and B. Alternatively, the temperature can be obtained directly from a calibration curve in the same optical path. Additionally, PIV/PLIF techniques require precise coordination between the laser plane and cameras, and when the tank height is significant, both laser penetration capability and camera field of view become limited. Cold water entering from the bottom inlet primarily concentrates its flow and mixing in the lower half of the tank. Therefore, during analysis, capturing only the lower half can avoid excessive differences in signal strength between the upper and lower sections, thereby improving the accuracy of velocity and temperature field data.

2.4. Experimental conditions

In order to investigate the transient flow characteristics of the horizontal circular cross buoyant jet at the inlet within a square water tank filled with uniform ambient fluid, the *Re* range of 940 $\leqslant Re \leqslant$ 3290 at the inlet was determined based on the typical flow rate range (227 L/h to 794 L/h) in practical engineering applications. Within this range, a total of 21 working conditions were designed for PIV and PLIF experimental studies, as shown in Table 3. At the beginning of the experiment, the water replenishment tank was continuously replenished with cold water of the same temperature and the same concentration of tracer particles into the cold water tank through the flow meter 1. At the same time, the cold water in the cold water tank with an initial temperature of T_0=20 °C flows into the hot water tank with a velocity of V_0 through the flow meter 2 with T_h=60 °C. The selection of T_0 and T_h is based on the typical inlet and outlet water temperatures in the storage tanks of solar water heating projects. Each experimental condition and its key parameters are listed in Table 3. It is noteworthy that the *Re* in the table refers to the inlet *Re*.

Table 3. List of PIV and PLIF experimental conditions and some key parameters

No.	*Re*(-)	*D*(m)	V_0(m/s)	T_h-T_0(°C)	h_0/l	PIV(*V*)	PLIF(*T*)
1	940	0.015	0.063	40±1	1/2		√
2	1410	0.015	0.094	40±1	1/2	-	√
3	1880	0.015	0.126	40±1	1/2		√
4-9	2350	0.015	0.157	40±1	1/2，1/3，1/8	√	√
10-15	2820	0.015	0.189	40±1	1/2，1/3，1/8	√	√
16-21	3290	0.015	0.220	40±1	1/2，1/3，1/8	√	√

3. Results and Analysis

3.1. Time average velocity field analysis

3.1.1 Time average velocity fields at different Re

To explore how different *Re* affect the flow characteristics of a jet, Figures 2(a) to 4(c) show the streamwise distributions of the time-averaged vertical velocity of the jet at *Re*=2350, 2820, and 3290 at h_0/l=1/2. Taking the velocity field distribution at the jet inlet with *Re*=2350 and initial velocity V_0=0.157m/s (Figure 2(a)) as an example, a shear layer forms upon jet entry into the water tank, triggered by velocity discrepancies between the jet and ambient fluid, this shear layer exhibits Kelvin-Helmholtz instability. As the jet continues to develop, the ambient fluid that is entrained in the fluid also increases, and the jet boundary gradually expands to both sides. Kelvin-Helmholtz instability progression enhances fluid entrainment and mixing. When the jet hits the wall of the tank, it rises to its maximum height along the wall and thenbegins to fall back, and the falling fluid continues to roll and entrain the surrounding ambient fluid, forming an obvious vortex structure. Vortex dimensions correlate with entrainment intensity, reflecting mixing between the jet and ambient fluid. Notably, as jet inlet velocity increases, the bilateral fluid penetration width grows, further indicating enhanced jet entrainment capacity and broader cold-hot water mixing zones at higher *Re*, attributable to more vigorous Kelvin-Helmholtz instability development. When the *Re* is low, viscous forces dominate the flow and suppress the growth of inherent Kelvin-Helmholtz instability in the shear layer. Although turbulent eddies and vortex structures still form due to instability, their spatial scales are smaller and their temporal evolution is more gradual compared to higher *Re* conditions. As *Re* increases, inertial forces amplify the instability, leading to the rapid development of larger-scale turbulence and coherent vortex structures that dominate the flow dynamics.

A comparison of Figs. 2(a)~(c) shows that the maximum vortex heights (h_v) formed after the jet rises along the opposite side of the tank are 65.6 mm, 96. mm, and 113. mm, respectively. 46.9% increase in h_v in Figure 2(b) compared to Figure 2(a), and 17.3% increase in h_v in Figure 2(c) compared to Figure

2(b), indicating that the magnitude of jet inlet *Re* has a significant effect on the fluid flow and mixing in the tank. As the *Re* increases, the fluid exhibits complex turbulence characteristics in the vortex, which also makes the mixing between hot and cold fluids more intense. In Figures 2(b) and 2(c) the height and intensity of the vortex increases as the *Re* increases. This further increases the mixing between the fluids. When the *Re* is low, viscous forces dominate the flow and the fluid flow is more stable and less likely to form turbulent and vortex structures. However, as the *Re* increases, the inertial force of the fluid gradually increases and the viscous force becomes relatively weaker, making the fluid flow unstable and more likely to form turbulence and vortex.

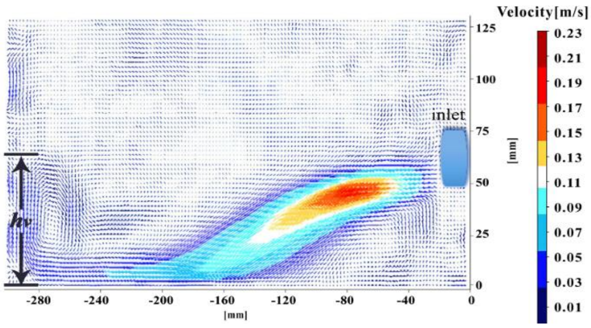

(a) *Re*=2350

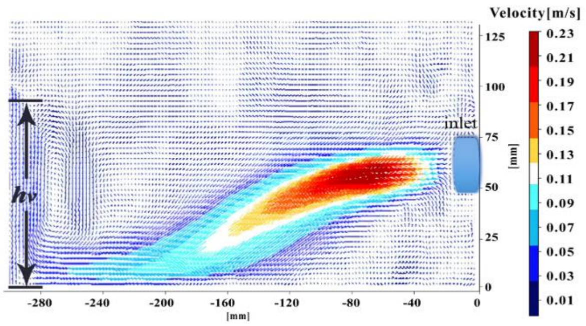

(b) *Re*=2820

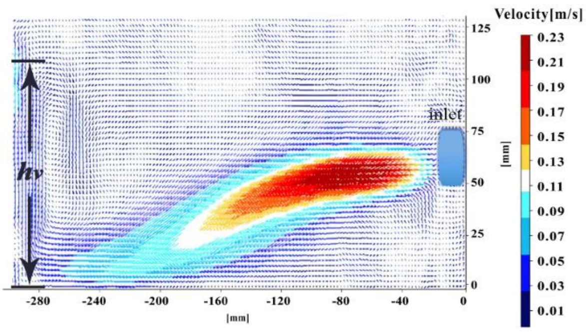

(c) *Re*=3290

Figure 2. Time average velocity vector diagram of a horizontal negative buoyant jet under different *Re*

3.1.2 Time-averaged velocity field at different outlet positions

When designing a hot water system, the position of the inlet and outlet of the storage tank can be different depending on the water consumption pattern. The position of the inlet and outlet will affect the degree of mixing of hot and cold water in the tank. Figure 3(a) and Figure 3(b) respectively show the time-averaged velocity fields in the vertical section of the inlet cross-section of the water tank under the jet *Re*=2820 and different hot water outlet ratios of h_0/l=1/2 and h_0/l=1/3.

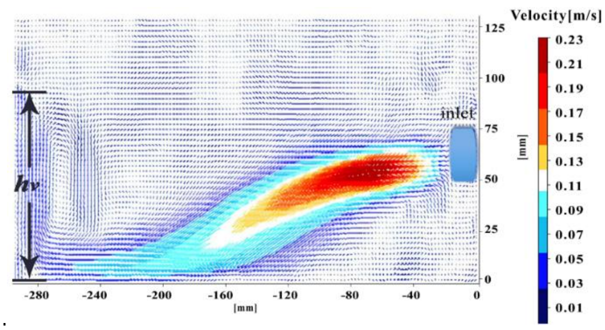

(a) *Re*=2820, h_0/l=1/2

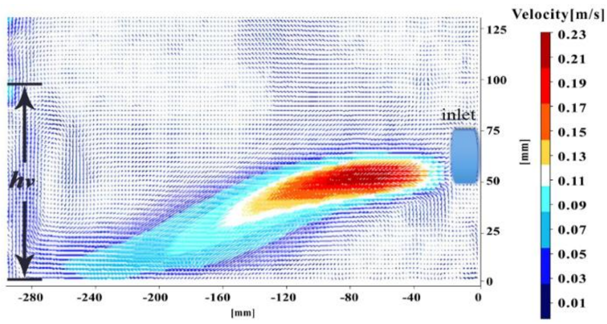

(b) *Re*=2820, h_0/l=1/3

Figure 3. Time average velocity vector diagram of a horizontal negative buoyant jet under different outlet

Comparing Figures 3(a) and (b) shows the jets have similar flow characteristics after mixing with hot water in the tank. In Figure 3(b), the jet requires an extended development length prior to fully impinging on the bottom wall within the interval [-240, -200] interval, owing to its elevated outlet position. As a result, the thickness of the jet within this zone is significantly thicker compared to Figure 3(a), reflecting the fact that the jet is entrained with more ambient fluid in this region and the mixing effect is more pronounced. However, in terms of the maximum height h_v of the jet, the value of h_v in Figure 3(b) is 96.6 mm, which is only 5.75% higher than the value of 91.4 mm in Figure 3(a).

3.2. Axial velocity distribution of jets

The distribution of axial velocities along the horizontal mean centerline of the jet, as shown in Figure 4(a)~(c), varies with different *Re* while maintaining a fixed outlet position. Compared to higher *Re* flows, the process of jet velocity decrease is smoother at low *Re*. This is attributed to the more significant effect of fluid viscous forces at low *Re*, which limits the momentum exchange and mixing between the jet and the ambient fluid. As the *Re* increases, the jet entrainment of the ambient fluid increases, which promotes the mixing of hot and cold water. The jet at high *Re* has stronger kinetic energy and momentum and can mix and exchange with the ambient fluid more effectively. As the jet develops, the curve tends to flatten, indicating that the jet velocity is lower at this time and mixing with the surrounding ambient fluid is weaker. Near the axial coordinate x=0.25~0.30, the jet rises to a maximum height and forms a vortex after hitting the tank wall, and then starts to fall back, and the entrainment and mixing of the jet with the ambient fluid is also further promoted by the ambient fluid entrainment and mixing of the falling fluid. In the uniform ambient fluid, the jet flow in the vertical section can be divided into three regions: the initial section of the jet, the transition section of the jet and the main section of the jet. The characteristics of the jet in these three regions are significantly different, not only in terms of flow velocity distribution, but also in terms of the size of the eddy formed and the ability to mix the ambient fluid. In the initial part of the jet, as the jet is just leaving the inlet, its velocity is greatest and mixing with the ambient fluid is weak. Therefore, the temperature gradient is greatest in this region. As the jet flows into the transition region, the velocity of the jet gradually decreases while mixing with the ambient fluid increases, resulting in a gradual increase in the diffusion range of the jet. Finally, the jet flows into the main section where the jet and ambient velocities become uniform and the mixing reaches an equilibrium state.

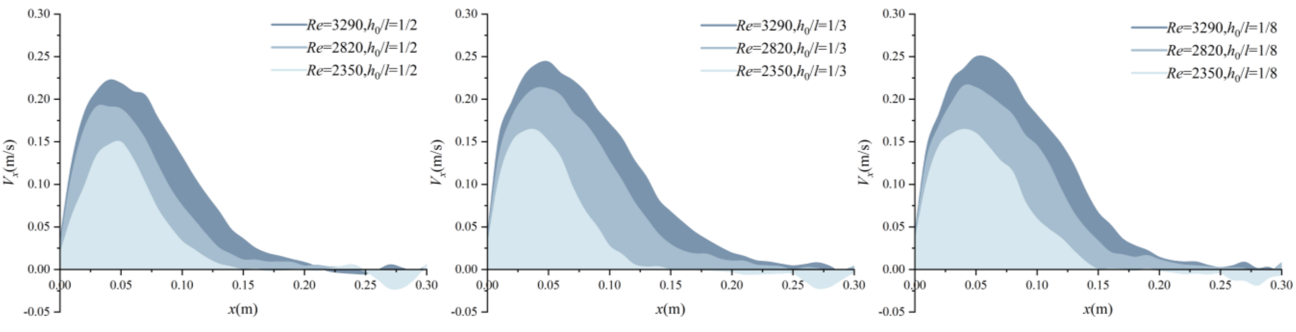

(a) h_0/l=1/2 (b) h_0/l=1/3 (c) h_0/l=1/8

Figure 4. The average axial velocity of the center line along the horizontal direction under different *Re*

3.3. Results and analysis of the PLIF experiment

3.3.1 Instantaneous temperature field of jet flows at different Re

Figure 5 presents an instantaneous PLIF image of a horizontal round cross-buoyant jet at the inlet of a square tank's central vertical plane (35.2 s), showing initial jet mixing. This initial mixing is crucial for forming subsequent temperature stratification or mixing states. Studying this stage can provide preliminary insights into the overall temperature field development and subsequent stratification behavior in the tank. At lower *Re*, the distribution of the low-temperature region in the jet zone is more concentrated. Conversely, at higher *Re*, the jet penetration range to expand, which intensifies mixing, resulting in an increased interface area between cold and hot water masses. The initial part of the jet maintains a low temperature, and as the jet develops, the temperature gradually begins to mix with the surroundings. As *Re* increases, the velocity differential and density contrast between the jet and surrounding fluid intensify, potentially enhancing Kelvin-Helmholtz Instability. This instability, in turn, contributes to more vigorous mixing and a more disordered temperature distribution within the fluid. Therefore, to optimize hot water extraction while maintaining the required water supply flow rate, reducing the inlet *Re* can effectively minimize the mixing of hot and cold water, allowing for greater removal of hot water.

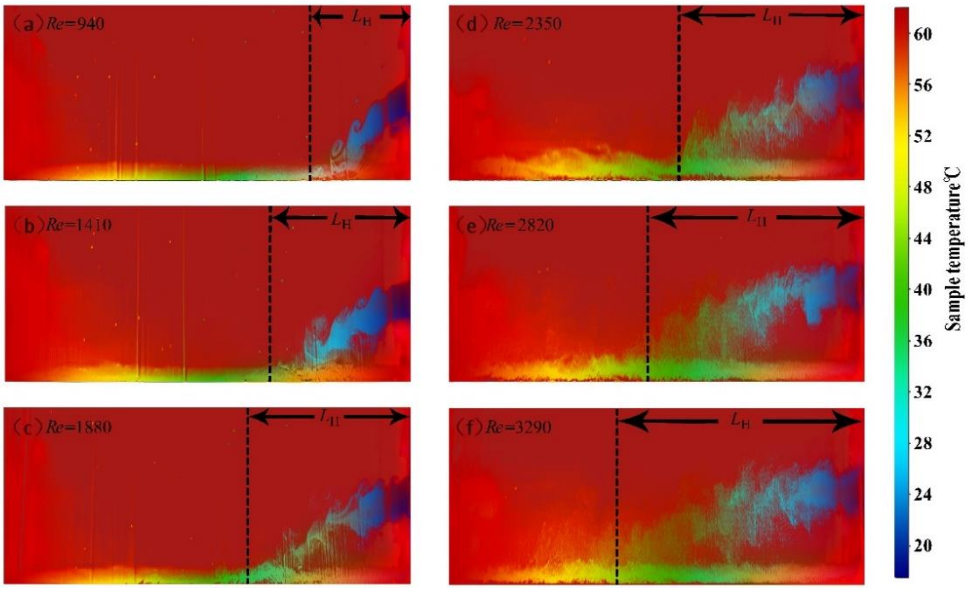

Figure 5. Diagram of instantaneous temperature field under different *Re* (vertical plane)

In Figure 5, we indicate the maximum jet penetration distance (L_H), defined as the ratio of the horizontal distance from the jet entry point to where it contacts the tank bottom, relative to the tank width. L_H directly reflects the jet's penetration capability within the square thermal storage tank. Data for L_H were collected across the range $940 \leqslant Re \leqslant 3290$. A linear model was used to describe the relationship between L_H and Re, as shown in Figure 6. The fitted equation is as follows:

$$L_H = 0.06362 + 0.000165Re \tag{3}$$

The equation indicates that as the *Re* increases, the inertial forces of the jet increasingly outweigh the viscous forces. The jet is more likely to maintain its initial velocity and direction, thus increasing its maximum penetration distance and intensifying the mixing of hot and cold water.

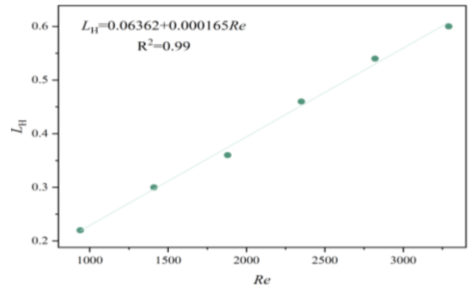

Figure 6. The fitting relationship between *Re* and L_H

3.3.2 Instantaneous temperature field of different hot water outlet jets

Figure 7 illustrates the instantaneous temperature field of the negatively buoyant jet on the vertical cross section at the water inlet in the tank at different h_0/l. A thorough examination of instantaneous images of the jet at 35.2 seconds post-processing reveals that, at the same *Re*, the diffusion lengths of the jet at different h_0/l are essentially consistent at the same moment. However, the distribution of the temperature field varies based on the outlet location. In Figure 7(a), when h_0/l=1/2, the initial temperature field of the cold water jet appears compact, with an indistinct thermal jump region. This is

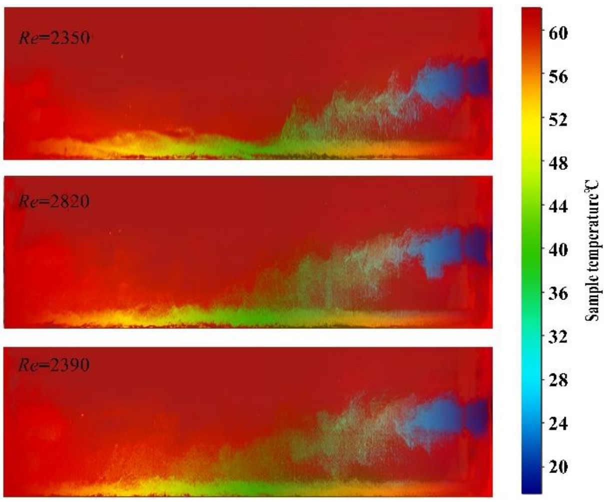

（a）h_0/l=1/2

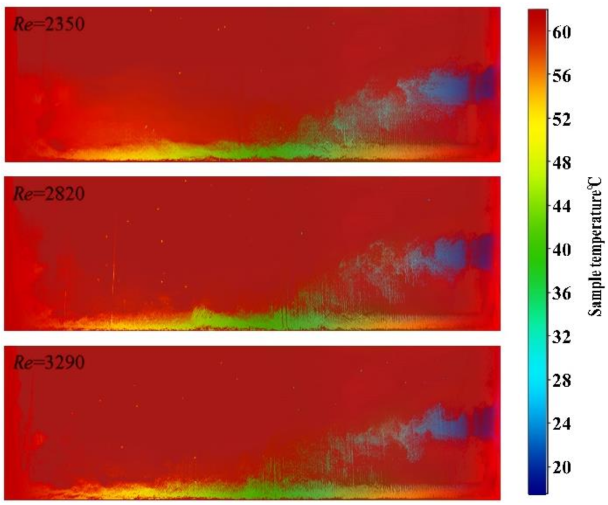

（b）h_0/l=1/3

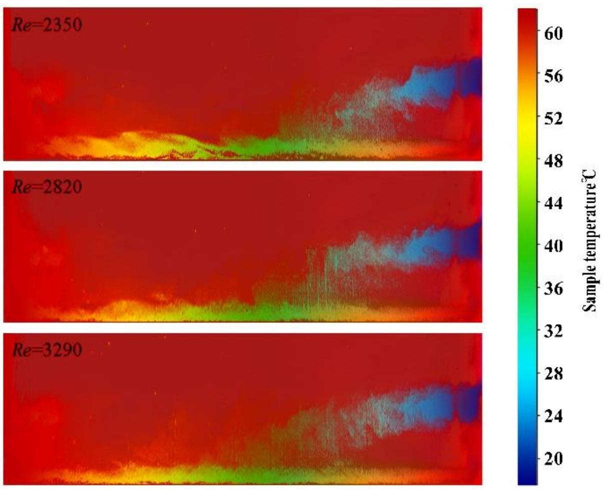

（c）h_0/l =1/8

Figure 7. Diagram of instantaneous temperature field under different outlet positions (vertical plane)

a typical thermal characteristic when the jet first exits the nozzle. As the jet develops downstream, the cold water with low temperature and high momentum has strong heat exchange with the ambient fluid, and the low-temperature water spreads rapidly in all directions in the hot water, resulting in a thermocline region that gradually decreases from the center outwards. A comparison of Figure 7(b) and (c) highlights the substantial changes in temperature field distribution associated with higher outlet positions of the jet. The higher outlet position promotes a stronger mixing between the jet and the ambient fluid. In Figure 7(b) and (c), the temperature difference between the core and edge regions of the jet is significantly reduced, resulting in a smoother and more homogeneous thermocline. Therefore, from a mixing reduction point of view, there is relatively less mixing in the core region of the jet when h_0/l=1/2.

4. Conclusion

In this study, the velocity and temperature fields of horizontal buoyant jets in a square tank model were measured using PIV/PLIF techniques under varying inlet *Re* and h_0/l. Flow parameters, including time-averaged velocity and instantaneous temperature fields, were obtained for different working conditions. The qualitative and quantitative analyses of the flow field parameters under different working cases were carried out, and the main conclusions are as follows:

(1) After the cold water flows from the inlet into the hot water tank, it is entrained and mixed with the high temperature ambient fluid by the effect of the jet. As the *Re* increases, the inertial force gradually dominates, resulting in a significant penetration range of the jet. At the same time, under the influence of gravity, the jet gradually bends downwards after the initial part and finally flows along the bottom of the tank.

(2) Due to the effect of the initial momentum of the jet, the *Re* increases, the jet temperature penetration range is larger, the jet accordingly produces more, finer, uneven sizes, uneven distribution of entrainment vortex, showing that in the stronger level of cross buoyant jet effect, the fluid in the tank at all times produces disorderly entrainment and mixing.

(3) The mixing phenomenon within the core region of the jet is relatively mild at the exit position h_0/l=1/2 case. When $940 \leqslant Re \leqslant 1880$, the boundary distinction between cold and hot water is more pronounced. When $2350 \leqslant Re \leqslant 3290$, the area of cold and hot water mixing increases, enhancing the mixing between the jet and the surrounding fluid.

Acknowledgment

This research was funded by the National Natural Science Foundation of China (12262036, 51969032) and by the National Science Foundation of Yunnan Province (grant number 202301AT070064). Experiments and simulations were conducted at Computational Fluid Mechanics and Heat Transfer Laboratory (CFMHTL) in Yunnan Normal University.

Nomenclature

A Intensity ratio
B Calibration parameters
h_0/l Ratio between the height of the top of the tank and the height of the tank at the shaft of the hot water outlet pipe
h_v Maximum vortex heights
L_H Highest advancement length
Re Reynolds number
R_f Fluorescence intensity
$R_{f,ref}$ Reference fluorescence intensity
T Temperature
T_{ref} Reference temperature
T_0 Cold water temperature
T_h Hot water temperature
V Velocity

Greek Letters

$\lambda_{a,max}$ Maximum absorption wavelength
$\lambda_{e,max}$ Maximum emission wavelength

Subscripts

a Absorption
e Emission
f Fluorescence
ref Reference

Abbreviations

PLIF Planar Laser Induced Fluorescence
PIV Particle Image VelocimetryReferences

References

[1] Sun, J., *et al.*, Experimental study of a large temperature difference thermal energy storage tank for centralized heating systems, *Thermal Science*, *22* (2018), 1B, pp. 613-621

[2] Milanovic, P., *et al.*, Dynamic modeling of a heating system using geothermal energy and storage tank, *Thermal Science*, *16* (2012), 3, pp. 947-953

[3] Li, J., *et al.*, Long-term performance of a solar water heating system with a novel variable-volume tank, *Renewable Energy*, *164* (2021), pp. 230-241

[4] Qin, Y., *et al.*, The effect of phase change material balls on the thermal characteristics in hot water tanks: CFD research, *Applied Thermal Engineering*, *178* (2020), 115557

[5] Li, Q., *et al.*, Thermocline dynamics in a thermally stratified water tank under different operation modes, *Applied Thermal Engineering*, *212* (2022), 118560

[6] Philippe, P., *et al.*, Penetration of a negatively buoyant jet in a miscible liquid, *Physics of Fluids*, *17* (2005), 5, 053601

[7] Qin, S., *et al.*, Velocity field and scalar field measurements of turbulent buoyant round jets in a two-layer stratified environment, *Nuclear Science and Engineering*, *194* (2020), 8-9, pp. 583-597

[8] van Berkel, J., *et al.*, Modelling of two-layer stratified stores, *Solar Energy*, *67* (1999), 1-3, pp. 65-78

[9] van Berkel, J., *et al.*, Thermocline dynamics in a thermally stratified store, *International Journal of Heat and Mass Transfer*, *45* (2002), 2, pp. 343-356

[10] González-Altozano, P., *et al.*, New methodology for the characterisation of thermal performance in a hot water storage tank during charging, *Applied Thermal Engineering*, *84* (2015), pp. 196-205

[11] Haddouche, M. R., *et al.*, Numerical approach and experimental investigation of a stratified hot water storage tank for domestic hot water production, *Results in Engineering*, *24* (2024), 103221

[12] El-Amin, M. F., *et al.*, Analysis of a turbulent buoyant confined jet modeled using realizable k–ε model, *Heat and Mass Transfer*, *46* (2010), 8-9, pp. 943-960

[13] El-Amin, M. F., *et al.*, Simulation of buoyancy-induced turbulent flow from a hot horizontal jet, *Journal of Hydrodynamics*, *26* (2014), 1, pp. 104-113

[14] El-Amin, M. F., *et al.*, Numerical simulation and analysis of confined turbulent buoyant jet with variable source, *Journal of Hydrodynamics*, *27* (2015), 6, pp. 955-968

[15] Chandra, Y. P., Matuska, T., Numerical prediction of the stratification performance in domestic hot water storage tanks, *Renewable Energy*, *154* (2020), pp. 1165-1179

[16] Assari, M. R., *et al.*, Numerical and experimental study of inlet-outlet locations effect in horizontal storage tank of solar water heater, *Sustainable Energy Technologies and Assessments*, *25* (2018), pp. 181-190

[17] Assaria, M. R., *et al.*, Experimental study on destruction of thermal stratification tank in solar collector performance, *Journal of Energy Storage*, *15* (2018), pp. 124-132

[18] Li, J., *et al.*, Thermal performance of a solar water tank with variable inlet/outlet under various charging strategies, *Applied Thermal Engineering*, *246* (2024), 122900

[19] Mingotti, N., *et al.*, The mixing of airborne contaminants by the repeated passage of people along a corridor, *Journal of Fluid Mechanics*, *903* (2020), A52

[20] Liu, F., *et al.*, Interactions of exhaled buoyant jet flow and human motion-induced airflow: An experiment study in a water tank, *Building and Environment*, *242* (2023), 110603

[21] Bruchhausen, M., *et al.*, Instantaneous measurement of two-dimensional temperature distributions by means of two-color planar laser induced fluorescence (PLIF), *Experiments in Fluids*, *38* (2004), 1, pp. 123-131

[22] Eghtesad, A., *et al.*, A state-of-the-art review on laser-induced fluorescence (LIF) method with application in temperature measurement, *International Journal of Thermal Sciences*, *196* (2024), 108686

Received: 11.01.2025.
Revised: 17.04.2025.
Accepted: 09.06.2025.